A Coordinating Control Strategy for Autothermal Fuel Reforming Systems

Jian Chen and Jing Sun, *Fellow, IEEE*

Abstract—In this paper, a control-oriented nonlinear model is developed for an autothermal reformer-based fuel process system. By trajectory planning for one of the system states, a coordinating control algorithm is proposed for the three input flow rates to track/regulate the temperature and hydrogen production of the autothermal reformer. Stability analysis is provided to show a local uniformly ultimately bounded tracking result. Simulation results illustrate the performance of the proposed control algorithm.

Index Terms—Autothermal reforming, coordinating control, dynamic modeling, fuel cells, fuel reforming technologies, nonlinear systems.

NOMENCLATURE

Symbol	Description
F	Faraday's constant $(\mathrm{C} \cdot \mathrm{mol}^{-1})$.
I_{st}	Fuel cell current (A).
R	Universal gas constant $(\mathrm{J} \cdot \mathrm{mol}^{-1} \cdot \mathrm{K}^{-1})$.
T	Temperature (K).
W	Mass flow $(\mathrm{g} \cdot \mathrm{s}^{-1})$.
c_p	Specific heat $(\mathrm{J} \cdot \mathrm{g}^{-1} \cdot \mathrm{K}^{-1})$.
U_{H_2}	Fuel utilization.
P	Pressure (Pa).
m	Mass (g).
M	Molar weight $(\mathrm{g} \cdot \mathrm{mol}^{-1})$.
V	Volume (m^3).
α	Orifice constant $(\mathrm{g} \cdot \mathrm{Pa} \cdot \mathrm{s}^{-1})$.
$x^{\mathrm{mix}}_{\mathrm{fuel}}$	Mass fraction of the fuel in the MIX.
x^{mix}_{st}	Mass fraction of the steam in the MIX.
n	Number of cells.
λ_{s2f}	Steam-to-fuel molar ratio.
λ_{o2f}	Oxygen-to-fuel molar ratio.
$g_{\mathrm{in}}, g_{\mathrm{out}}$	Enthalpy flows for the inlet and outlet of the ATR $(\mathrm{J/s})$.
$n_{(\cdot)}$	Molar flow of species $(\mathrm{mol/s})$.
y	Hydrogen mass flow $(\mathrm{g/s})$.
$\bar{n}_{\mathrm{H}_2}$	Hydrogen production per mole of the fuel.

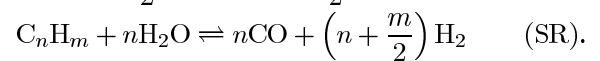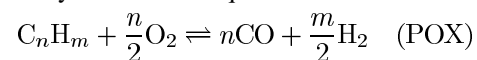*Sub(Super) Scripts:*

asm	Air supply manifold.
atr	Autothermal reformer.
fuel	Fuel.
mix	Mixer.
st	Steam.

J. Chen was with the Department of Naval Architecture and Marine Engineering, University of Michigan, Ann Arbor, MI 48109 USA. He is now with IdaTech LLC, Bend, OR 97701 USA (e-mail: jianc@umich.edu).

J. Sun is with the Department of Naval Architecture and Marine Engineering, University of Michigan, Ann Arbor, MI 48109 USA.
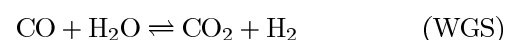
I. INTRODUCTION

FUEL CELLS (FCs), integrated with fuel reforming technologies, are promised to be very efficient for converting fuel chemical energy into electricity. For example, high temperature solid oxide fuel cells (SOFC), when coupled with a gas turbine (GT) cycle, can achieve efficiency up to 70%[1], [2]. Steam reforming (SR), partial oxidation (POX), and autothermal reforming (ATR) are three commonly used reforming technologies that can provide the hydrogen rich fuel feed stock for SOFC [3]–[5] or proton exchange membrane fuel cell (PEM FC) [6] applications. While the steam reforming and partial oxidation both have their own advantages over the other, the basic idea of the autothermal reforming is that both the endothermic steam reforming reaction and the exothermic POX reaction occur together, so that no heat needs to be supplied to (as for the steam reforming) or removed from (as the partial oxidation reforming) the system [5]. Another advantage of the autothermal reforming is that less steam is needed compared with conventional steam reforming [5].

For a given generic hydrocarbon fuel $\mathrm{C}_n\mathrm{H}_m$, the two main reactions associated with the autothermal reforming process can be described by the reaction equations as follows:

$$\mathrm{C}_n\mathrm{H}_m + \frac{n}{2}\mathrm{O}_2 \rightleftharpoons n\mathrm{CO} + \frac{m}{2}\mathrm{H}_2 \quad \text{(POX)}$$

$$\mathrm{C}_n\mathrm{H}_m + n\mathrm{H}_2\mathrm{O} \rightleftharpoons n\mathrm{CO} + \left(n + \frac{m}{2}\right)\mathrm{H}_2 \quad \text{(SR)}.$$

The other main reactions, namely the water-gas shift reaction (WGS) and the methane formation (MF), also proceed simultaneously and yield a gas composition [7] as follows:

$$\mathrm{CO} + \mathrm{H}_2\mathrm{O} \rightleftharpoons \mathrm{CO}_2 + \mathrm{H}_2 \quad \text{(WGS)}$$

$$\mathrm{CO} + 3\mathrm{H}_2 \rightleftharpoons \mathrm{CH}_4 + \mathrm{H}_2\mathrm{O}. \quad \text{(MF)}$$

The control objective of the ATR fuel reforming systems is to produce enough hydrogen efficiently to support the fuel cell load while maintaining the operation temperature of the reactors within their safe range to avoid carbon deposit or crack formation. Tsourapas *et al.* [8] presented a lumped parameter dynamic model of an autothermal JP-5 reformer using ordinary differential equations. A separator membrane (SEP) is incorporated to extract the hydrogen from the reformate flow. The system with open loop control is simulated and analyzed with respect to the SEP operation. As stated in [8], feedback control is required when uncertainties (such as system parameter uncertainty, measurement noise, and unmodeled physical phenomena including spatial distributions of temperature, pressure, species concentration, and current along the flow channel, the slow steam reforming reaction etc.) are present. It is therefore essential to assure that the control system is robust with respect to the system uncertainties. Papadias *et al.* [9] developed a partial differential equation (PDE) mathematical model for an ATR fuel processor to study the transient response of the reactor for gasoline reforming. To use PDE models for control development, usually further work needs to be done to make the model amenable to existing design tools. By linearizing the Catalytic Partial Oxidation (CPOX) fuel reforming system at the operating point, Pukrushpan *et al.* [10], [11] proposed a decentralized control algorithm and a multivariable control algorithm to regulate both the hydrogen mole fraction and the reformer temperature. As claimed in [10], the interactions in the plant limit the performance of the decentralized controller. The linear quadratic method is applied to design the controller gains for the multivariable control algorithm. As summarized in [12], a linear controller may exhibit significant performance degradation or even instability in the presence of model uncertainties while good nonlinear control designs can deal with model uncertainties and may be simpler and more intuitive than their linear counterparts. An example of the drawback of a linear controller for autothermal reforming is given in [13].

Motivated by the advantages of the nonlinear control, a nonlinear coordinating control is proposed in this paper for an autothermal fuel reforming system. By leveraging the results from [8], a dynamic model of the ATR system is developed with air, fuel, and steam flow rates as the inputs and the hydrogen mass flow rate and the ATR temperature as the outputs. Based on the nonlinearities and the structure of the dynamic model of the fuel reforming system, a desired trajectory is designed for the pressure of the air supply manifold (ASM) which is utilized as a virtual control input to the ATR temperature dynamic system. A pseudo-inverse technique is then applied along with the desired ASM pressure to coordinate (for coordinating control technique, see [14]) the three input flow rates to control both the hydrogen mass flow rate and the temperature of the ATR. The motivation to extend the ATR temperature regulation control to tracking control is to provide an auxiliary control term, the desired ATR temperature trajectory, that can be used to achieve desired ATR performance for different operating conditions. By incorporating the safety constraint, standard offline optimization or online extremum seeking algorithms (please refer to [15] for some extremum seeking algorithms) can be utilized to gen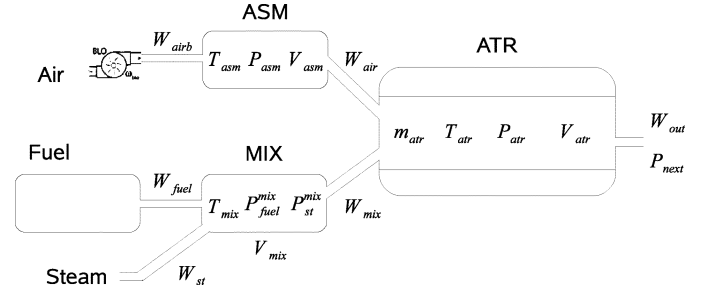erate the desired trajectory for the ATR temperature to maximize the efficiency of hydrogen production for different load conditions, thereby assuring safe and efficient operation of the reforming system.

This paper is organized in the following manner. In Section II, the ATR fuel reforming system model is developed. Section III details the error system development, control design, and stability analysis. Simulation results are provided in Section IV to illustrate the performance of the proposed control algorithm. Concluding remarks are given in Section V.

II. MODEL DEVELOPMENT

In this section, we present a control-oriented model which will be used to facilitate the model-based control design in the sequel. The main goal for this modeling effort is to develop a simple, yet useful, representation of the system that captures the key dynamics of the underlying physical systems. Another key consideration of the control-oriented model is that the resulting model should be amenable to existing design tools. It should be noted that the model developed in this section differs from those design-oriented model (such as those reviewed in [16]) in the level of details, due to the different functions that these two types of models intended to serve. In [17], a in-depth study was carried out to evaluate the validity of a low order model by comparing to a detailed model with kinetic reactions, spatial distributions of temperature, current, and species concentration, and concluded that the low order control-oriented model can be very effective in representing the dynamic behavior of the system that critical to control designs.

A simplified ATR fuel process system considered in this paper includes an air supply manifold, a mixer (MIX), and an autothermal reforming unit as shown in Fig. 1. In this model, we assume that the temperatures of the air supply manifold and the mixer can be well controlled. From the fuel processing system point of view, these two temperatures are known constants. The control inputs are the mass flows of air, fuel, and steam. Standard backstepping techniques can be used to compensate for the dynamics of fuel and steam valves and the air blower when actuator dynamics are taken into account. The control outputs are the hydrogen mass flow rate and the reformer temperature.

A. ASM Model

With a constant temperature of the air supply manifold, the pressure dynamics in the air supply manifold can be expressed as follows [10], [18]

$$\frac{dP_{\mathrm{asm}}}{dt} = \frac{RT_{\mathrm{asm}}}{M_{\mathrm{air}}V_{\mathrm{asm}}}(W_{\mathrm{airb}} - W_{\mathrm{air}}) \qquad (1)$$

Fig. 1. Simplified ATR fuel processing system scheme.

where R is the universal gas constant, P_{asm}, T_{asm}, V_{asm} are the pressure, temperature, and volume of the air supply manifold, respectively, M_{air} is the molar mass of air, W_{airb}, W_{air} denote the mass flow rates of the ASM inlet and outlet, respectively. W_{air} can be obtained from a linearized form of the sub-critical nozzle flow equation [10] as follows:

$$W_{air} = \alpha_a(P_{asm} - P_{atr}) \qquad (2)$$

where P_{atr} denotes the pressure of the ATR, α_a is the orifice constant of the ASM outlet, which depends on the orifice size, geometry, shape, etc.

B. Mix Model

With a constant temperature of the mixer, the partial pressure of the fuel and the steam inside the mixer, denoted as P_{fuel}^{mix}, P_{st}^{mix}, respectively, can be expressed as follows:

$$\frac{dP_{fuel}^{mix}}{dt} = \frac{RT_{mix}}{M_{fuel}V_{mix}} \left(W_{fuel} - x_{fuel}^{mix}W_{mix} \right)$$
$$\frac{dP_{st}^{mix}}{dt} = \frac{RT_{mix}}{M_{st}V_{mix}} \left(W_{st} - x_{st}^{mix}W_{mix} \right) \qquad (3)$$

where T_{mix}, V_{mix} are the temperature and volume of the mixer, respectively, W_{fuel}, W_{st} denote the mass flow rates of the fuel inlet and the steam inlet, respectively, M_{fuel}, M_{st} are the molar mass of fuel and steam, respectively, W_{mix}, denoted as the mass flow rate of the mixer outlet, can be obtained from the linearized nozzle flow equation as follows:

$$W_{mix} = \alpha_m(P_{fuel}^{mix} + P_{st}^{mix} - P_{atr}) \qquad (4)$$

where α_m is the orifice constant of the mixer outlet. In (3), x_{fuel}^{mix}, x_{st}^{mix} are the mass fractions of the fuel and the steam in the MIX, respectively, and are calculated by

$$x_{fuel}^{mix} = \frac{1}{1 + \frac{M_{st}P_{st}^{mix}}{M_{fuel}P_{fuel}^{mix}}}, \quad x_{st}^{mix} = \frac{1}{1 + \frac{M_{fuel}P_{fuel}^{mix}}{M_{st}P_{st}^{mix}}}. \qquad (5)$$

C. ATR Model

Based on the ideal gas law, the pressure dynamics of P_{atr} can be expressed as follows:

$$\frac{dP_{atr}}{dt} = \frac{RT_{atr}}{M_{atr}V_{atr}} \left(W_{air} + W_{mix} - W_{out} \right) + \frac{P_{atr}}{T_{atr}}\frac{dT_{atr}}{dt} \qquad (6)$$

where T_{atr}, V_{atr} denote the temperature and volume of the ATR, respectively, and M_{atr} denotes the average molar mass of the gas inside the ATR. In (6), W_{out}, denoted as the mass flow rate of the ATR outlet, can be obtained from the linearized nozzle flow equation as follows

$$W_{out} = \alpha_{out}(P_{atr} - P_{next}) \qquad (7)$$

where α_{out} denotes the orifice constant of the ATR outlet, and P_{next} denotes the downstream pressure of the ATR.

Remark 1: Usually, the average molar mass is utilized in the fuel cell research community to simplify the model [10]. In our simulation, the change of the average molar mass M_{atr} is not

significant during the transient (less than 2% for the range of simulation conditions we evaluated). More precisely, the dynamics of P_{atr} can be expressed as follows:

$$\frac{dP_{atr}}{dt} = \frac{RT_{atr}}{M_{atr}V_{atr}} \left(W_{air} + W_{mix} - W_{out} \right) + \frac{P_{atr}}{T_{atr}}\dot{T}_{atr}$$
$$- \frac{P_{atr}}{M_{atr}}\dot{M}_{atr}. \qquad (8)$$

In (8), it is clear that $(P_{atr}/M_{atr})\dot{M}_{atr}$ is an additive uncertainty to the model in (6). Within the scope of our work, we are only interested in a compact space and this additive uncertainty can be modeled as a bounded term. In the subsequence analysis, we will show that our proposed algorithm is robust to bounded additive uncertainties.

Based on the assumption that the reactors are well insulated and therefore the heat losses to the environment can be neglected, the temperature dynamics of the ATR can be expressed as follows [8]:

$$\frac{dT_{atr}}{dt} = \frac{1}{m_c c_c} \left(g_{in}(\cdot) - g_{out}(\cdot) \right) \qquad (9)$$

where m_c, c_c denote the combined mass and the combined thermal capacity of the ATR. In (9), $g_{in}(\cdot)$, $g_{out}(\cdot)$ are defined as total enthalpy flows for the inlet and outlet of the ATR, respectively. The term g_{out} in (9) does not only contain the enthalpy flux out of the reactor but also the heat production by the reaction. $g_{out}(\cdot)$ depends on the temperature of the ATR, the outlet composition and the flow rate while the outlet composition depends on the temperature of the ATR, the steam-to-fuel molar ratio, and the oxygen-to-fuel molar ratio. To simplify the problem, we ignore the molar ratio distribution along the ATR channel and the chemical reaction effects on the steam-to-fuel ratio and the oxygen-to-fuel ratio. The steam-to-fuel molar ratio λ_{s2f} and the oxygen-to-fuel molar ratio λ_{o2f} are assumed only depend on the input flows as follows:

$$\lambda_{s2f} \triangleq \frac{n_{H_2O}}{n_{C_nH_m}} = \frac{M_{fuel}}{M_{st}} \cdot \frac{x_{st}^{mix}}{x_{fuel}^{mix}}$$
$$\lambda_{o2f} \triangleq \frac{n_{O_2}}{n_{C_nH_m}} = \frac{0.2095M_{fuel}}{M_{O_2}} \cdot \frac{W_{air}}{x_{fuel}^{mix}W_{mix}} \qquad (10)$$

where $n_{(\cdot)}$ is the molar flow of species $(\cdot)$. Based on (2), (4), (5), and (10), it is clear that $g_{out}(\cdot)$ is a function of $P_{asm}, P_{fuel}^{mix}, P_{st}^{mix}, P_{atr}, T_{atr}$ and can be written as $g_{out}\left(P_{asm}, P_{fuel}^{mix}, P_{st}^{mix}, P_{atr}, T_{atr} \right)$. The chemical kinetic reactions are assumed faster than the other dynamics, such as the thermal and gas exchange dynamics of the system. Therefore the chemical reactions are always assumed to reach their equilibrium instantly. Precalculated lookup tables generated by GasEq software (a chemical equilibrium program which utilizes the Gibbs energy minimization algorithm to calculate the reaction products, see http://www.gaseq.co.uk) are utilized to map the ATR products to its inlet conditions, namely, T_{atr}, λ_{s2f}, and λ_{o2f}. For our case, Diesel Oil No. 2 fuel is used as the fuel for autothermal reforming. We approximate Diesel Oil No. 2 fuel with average formula $C_{12}H_{26}$[19]. Fig. 2 shows an example of the precalculated maps for the hydrogen production
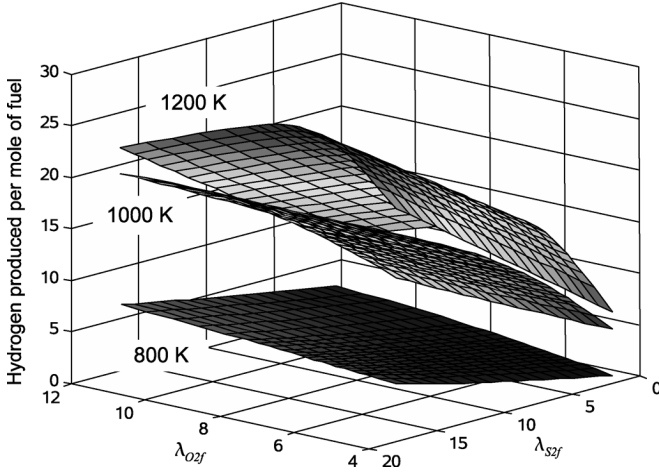
Fig. 2. ATR hydrogen production per mole of Diesel Oil No. 2 fuel at 800, 1000, and 1200 K.

Fig. 3. Smoothed ramp function with $a = 1$ and $h = 1$.

per mole of Diesel Oil No. 2 fuel at three different temperatures. With the fixed compositions and temperatures of the ATR inlets, the enthalpies of the ATR inlets are proportional to the inlet flow rates. Therefore, $g_{in}(\cdot)$ can be simply expressed in terms of flow rates of air, fuel, and steam as follows:

$$g_{in} = K_{air}(P_{asm} - P_{atr}) + K_{fuel}x_{fuel}^{mix}W_{mix} + K_{st}x_{st}^{mix}W_{mix} \quad (11)$$

where (2) was utilized. In (11), $K_{air}, K_{fuel}, K_{st}$ are constants which depend on the corresponding inlet flow temperatures (K_{air} also depends on α_a). Based on (4), (5), and (11), it is clear that $g_{in}(\cdot)$ is a function of $P_{asm}, P_{fuel}^{mix}, P_{st}^{mix}, P_{atr}$ and can be written as $g_{in}\left(P_{asm}, P_{fuel}^{mix}, P_{st}^{mix}, P_{atr}\right)$.

Hydrogen mass flow y from the ATR can be calculated as follows:

$$y = \frac{M_{H_2}x_{fuel}^{mix}W_{mix}\bar{n}_{H_2}}{M_{fuel}} \quad (12)$$

where $\bar{n}_{H_2}(\lambda_{s2f}, \lambda_{o2f}, T_{atr})$ is the hydrogen production per mole of fuel, M_{H_2} denotes the molar mass of H_2. The rate of hydrogen reacted in the fuel cell is a function of stack current, I_{st}, through the electrochemistry principle [5]. Therefore, the desired hydrogen mass flow rate, denoted by $y_d(t)$, can be obtained through the following relationship[1]

$$y_d = \frac{M_{H_2}nI_{std}}{2U_{H_2}F} \quad (13)$$

where F denotes the Faraday's constant, n denotes the number of the fuel cell stack, U_{H_2} denotes the hydrogen utilization of the fuel cell stack which is regarded as a constant in our model and $0 < \epsilon < U_{H_2} < 1$, $I_{std}(t)$ is a smoothed version of $I_{st}(t)$ with $I_{std}(t), \dot{I}_{std}(t)$ bounded. From (13), it is clear that $y_d(t), \dot{y}_d(t)$ are bounded.

---

[1]With a DC/DC converter connected to the fuel cell stack, stack current demand, instead of the power load demand, is normally utilized as the system input. As [21] pointed out, the current is not a directly manipulable input variable. For this case, the desired hydrogen mass flow rate y_d can be related to power load demand directly based on the low heating value of the fuel with a scale factor of the fuel cell system efficiency
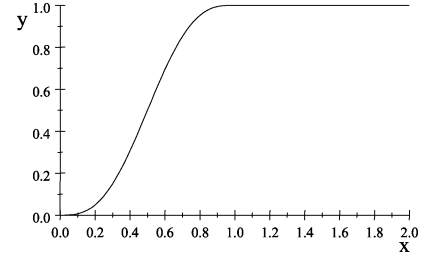
Remark 2: To smooth the current demand, we utilize the following function (In this remark, x and y denote the input and the output of the function, respectively)

$$y = \begin{cases} 0, & \text{if } x < 0 \\ \frac{a}{h}\left(x - \frac{h}{2\pi}\sin(2\pi\frac{x}{h})\right), & \text{if } 0 \leq x \leq h \\ a, & \text{if } h < x \end{cases} \quad (14)$$

where h is a time delay constant, and a is the magnitude of the current change. Fig. 3 shows one example of the smoothed ramp function. From (14), it is clear that the first and the second derivatives of the ramp function are zero at both $x = 0$ and $x = h$. This property allows us to include the $\dot{I}_{std}(t)$ term in the control inputs without introducing spikes to the closed-loop system at the time of the load changes. The time delay in the ramp function serves as a current rate limiter which can prevent hydrogen starvation [20]. I_{st} is the actual current that is required to draw from the fuel cell system to meet the power demand. In case of $I_{st} \neq I_{std}$, a battery pack or supercapacitor can be integrated with the fuel cell system to form a fuel cell-battery (or supercapacitors) based auxiliary power unit system. A DC/DC converter performs the function of voltage regulation as well as the power coordinating control. With the DC/DC converter and the battery pack (or supercapacitors), a smoothed current demand will be drawn from the fuel cell system and the actual current demand I_{st} can be met by drawing the current $(I_{st} - I_{std})$ from the battery pack (or supercapacitors).

D. Control Oriented Model

From (1)–(4), (6), (7), and (9), the control oriented model can be written in a compact form as follows:

$$\dot{X} = f(X, u) \quad (15)$$

where

$$X(t) \triangleq \begin{bmatrix} x_1(t) & x_2(t) & x_3(t) & x_4(t) & x_5(t) \end{bmatrix}^T$$
$$= \begin{bmatrix} P_{asm} & P_{fuel}^{mix} & P_{st}^{mix} & P_{atr} & T_{atr} \end{bmatrix}^T$$
$$u(t) \triangleq \begin{bmatrix} u_1(t) & u_2(t) & u_3(t) \end{bmatrix}^T$$
$$= \begin{bmatrix} W_{airb}(t) & W_{fuel}(t) & W_{st}(t) \end{bmatrix}^T$$

and $f(X, u)$ are defined as follows:

$$f(X, u) = \begin{bmatrix} b_1u_1 + \phi_1(x_1, x_4) \\ b_2u_2 + \phi_2(x_2, x_3, x_4) \\ b_3u_3 + \phi_3(x_2, x_3, x_4) \\ \phi_4(x_1, x_2, x_3, x_4, x_5) \\ \phi_5(x_1, x_2, x_3, x_4, x_5) \end{bmatrix}$$

and b_i, $\phi_i(t)$ $\forall i = 1, 2, \ldots, 5$, are defined as follows:

$$b_1 = \frac{RT_{\text{asm}}}{M_{\text{air}}V_{\text{asm}}}$$

$$b_2 = \frac{RT_{\text{mix}}}{M_{\text{fuel}}V_{\text{mix}}}$$

$$b_3 = \frac{RT_{\text{mix}}}{M_{st}V_{\text{mix}}}$$

$$b_4 = \frac{R}{M_{\text{atr}}V_{\text{atr}}}$$

$$b_5 = \frac{1}{m_c c_c}$$

$$\phi_1 = -b_1\alpha_a(P_{\text{asm}} - P_{\text{atr}})$$

$$\phi_2 = -b_2 x_{\text{fuel}}^{\text{mix}} W_{\text{mix}}$$

$$\phi_3 = -b_3 x_{st}^{\text{mix}} W_{\text{mix}}$$

$$\phi_4 = b_4 T_{\text{atr}} (W_{\text{air}} + W_{\text{mix}} - W_{\text{out}}) + \frac{P_{\text{atr}}}{T_{\text{atr}}}\phi_5$$

$$\phi_5 = b_5 (g_{\text{in}} - g_{\text{out}}).$$

After taking the time derivative of (12), the dynamics of $y(t)$ can be expressed as follows:

$$\dot{y} = [\, b_1\frac{\partial y}{\partial x_1} \quad b_2\frac{\partial y}{\partial x_2} \quad b_3\frac{\partial y}{\partial x_3}\,] u + N_1(t) \quad (16)$$

where $N_1(t) \triangleq \sum_{i=1}^{5}(\partial y/\partial x_i)\phi_i$ and $(\partial y/\partial x_i)$ $\forall i = 1, 2, \ldots, 5$, are the sensitivities of the hydrogen mass flow rate to the pressures of the system and the ATR temperature (see Appendix A for the expressions of $\partial y/\partial x_i$). To calculate $\partial y/\partial x_i$, the precalculated lookup table $\bar{n}_{\text{H}_2}$ is utilized to calculate $\partial\bar{n}_{\text{H}_2}/\partial\lambda_{o2f}$, $\partial\bar{n}_{\text{H}_2}/\partial\lambda_{s2f}$, and $\partial\bar{n}_{\text{H}_2}/\partial T_{\text{atr}}$. By fixing the values for two variables out of λ_{s2f}, λ_{o2f}, and T_{atr}, analytical expressions of $\bar{n}_{\text{H}_2}$ as functions of the rest variable out of λ_{s2f}, λ_{o2f}, and T_{atr} can be obtained using standard spline function in MATLAB. By taking the derivative of the resulting expressions, three lookup tables can be obtained for $\partial\bar{n}_{\text{H}_2}/\partial\lambda_{o2f}$, $\partial\bar{n}_{\text{H}_2}/\partial\lambda_{s2f}$, and $\partial\bar{n}_{\text{H}_2}/\partial T_{\text{atr}}$. In (15) and (16), all the states $P_{\text{asm}}(t)$, $P_{\text{fuel}}^{\text{mix}}(t)$, $P_{st}^{\text{mix}}(t)$ (measured by special sensors or estimated by some observers [22]), $P_{\text{atr}}(t)$, and $T_{\text{atr}}(t)$ are assumed to be measurable, and $y(t)$ can be calculated by (12). The fifth-order dynamic model developed in this section is mainly developed to facilitate the control design, therefore it has been intentionally kept simple and low order. The assumptions that have been made in this modeling work (such as the ideal gas law, instantaneous chemical reactions, etc.) are similar to those made in control literatures [18], [23] as well as in commercial software packages.[2] The model derived using the assumptions and approximations is suitable for the derivation of the control strategy. But it is worth to point out that, those assumptions are not based on first principles, and therefore they may not be totally correct from a physical point of view.

The validity of those low order model has been studied in several publications, such as [17] and [18], where the dynamic responses of the low-order models are compared with more detailed high order models or experimental results and the performance of the controller designed based on the low order model

is evaluated with high fidelity models or experimental results. However, the unmodeled physical phenomena, such as spatial distributions of temperature, pressure, species concentration and current along the flow channel, the slow steam reforming reaction, etc., could lead to unmodeled dynamics. It is therefore essential to assure that the control system is robust with respect to the unmodeled dynamics.

III. CONTROL DEVELOPMENT

From (15), it is clear that $T_{\text{atr}}(t)$ can only be controlled through the system states $x(t) \triangleq [\, x_1 \quad x_2 \quad x_3 \quad x_4 \quad x_5\,]^T$ while $P_{\text{asm}}(t)$, $P_{\text{fuel}}^{\text{mix}}(t)$, and $P_{st}^{\text{mix}}(t)$ can be controlled by $u(t)$ directly. Since $P_{\text{fuel}}^{\text{mix}}(t)$ and $P_{st}^{\text{mix}}(t)$ are coupled to each other and $P_{\text{asm}}(t)$ can be controlled more independently, we propose a coordinating control strategy for $u(t)$ which drives the hydrogen mass flow rate $y(t)$ to $y_d(t)$ and $P_{\text{asm}}(t)$ to follow a desired ASM pressure trajectory $\phi_6(t)$. $\phi_6(t)$ is designed such that $T_{\text{atr}}(t)$ tracks a desired ATR temperature when $P_{\text{asm}}(t)$ follows $\phi_6(t)$ ($\phi_6(t)$ to be defined later). To characterize the open-loop error dynamics, three tracking errors are defined as follows:

$$e_1 \triangleq P_{\text{asm}} - \phi_6, \quad e_2 \triangleq y - y_d, \quad e_3 \triangleq T_{\text{atr}} - T_{\text{atr}}^* \quad (17)$$

where $T_{\text{atr}}^*(t) \in \mathbb{R}$ is the desired ATR temperature. Here we unify the temperature regulation and temperature tracking problems together. For the case that $\dot{T}_{\text{atr}}^* \equiv 0$, our algorithm will regulate the temperature of the ATR to a desired setpoint. For the case that $\dot{T}_{\text{atr}}^* \neq 0$, our algorithm will track a desired temperature trajectory to facilitate system start-up, shut-down, and the ATR temperature setpoint change operations.

The desired ASM pressure trajectory $\phi_6(t)$ provides an intermediate control goal for the three input flow rates. When this intermediate goal is achieved, the ATR temperature will automatically track the desired ATR temperature. The desired ATR temperature $T_{\text{atr}}^*(t)$ can be set to maximize the efficiency of hydrogen production (the selection for $T_{\text{atr}}^*(t)$ is out of the scope of this paper).

For this overactuated system (driving $e_1(t)$ and $e_2(t)$ to zero or close to zero by three control input flow rates note that $e_3(t) \to 0$ will be achieved when $e_2(t) \to 0$), we propose a coordinating control strategy for the three input flow rates based on a pseudo-inverse technique which is commonly used in redundant robot manipulations. In Section III-B, a stability analysis is provided to show that the proposed algorithm achieves local uniformly ultimately bounded tracking.

A. Coordinating Control Design

Based on the structure of (9), (11), and the desired closed-loop dynamics in the following section, $\phi_6(t)$ is designed as follows:

$$\phi_6(t) \triangleq P_{\text{atr}}(t) + \frac{1}{K_{\text{air}}b_5}\left(-k_{\text{atr}}(T_{\text{atr}} - T_{\text{atr}}^*) + \dot{T}_{\text{atr}}^*\right)$$
$$- \frac{1}{K_{\text{air}}}\left(K_{\text{fuel}}x_{\text{fuel}}^{\text{mix}}W_{\text{mix}} + K_{st}x_{st}^{\text{mix}}W_{\text{mix}}\right) \quad (18)$$

where k_{atr} is a positive control gain which will be designed in the subsequent stability analysis. The first term in (18) is utilized to cancel P_{atr} in (11) and the third term in (18) is utilized to

cancel the second term and the third term in (11). The second term in (18) is utilized to get the desired closed loop dynamics.

After taking the time derivative of the first equation in (17), the dynamics of $e_1(t)$ can be expressed as follows

$$\dot{e}_1 = [\, b_1 \quad -b_2 \frac{\partial \phi_6}{\partial x_2} \quad -b_3 \frac{\partial \phi_6}{\partial x_3} \,] u + N_2 \tag{19}$$

where (15) was utilized and $N_2 \triangleq \phi_1 - \sum_{i=2}^{5} (\partial \phi_6 / \partial x_i) \phi_i$ and $\partial \phi_6 / \partial x_i \in \mathbb{R} \ \forall \ i = 2, 3, 4, 5$, are the sensitivities of the desired ASM pressure trajectory to the other states of the system (see Appendix B for the expressions of $\partial \phi_6 / \partial x_i$). After taking the time derivative of the second equation in (17), the dynamics of $e_2(t)$ can be expressed as follows:

$$\dot{e}_2 = [\, b_1 \frac{\partial y}{\partial x_1} \quad b_2 \frac{\partial y}{\partial x_2} \quad b_3 \frac{\partial y}{\partial x_3} \,] u + N_1(t) - \dot{y}_d \tag{20}$$

where (15) was utilized. From (19) and (20), the open-loop dynamics for $e_1(t)$, $e_2(t)$ can be expressed in a compact form as follows:

$$\begin{bmatrix} \dot{e}_1 \\ \dot{e}_2 \end{bmatrix} = Bu + N \tag{21}$$

where $N(t) \triangleq [\, N_2 \quad N_1 - \dot{y}_d \,]^T \in \mathbb{R}^2$ and $B(t) \in \mathbb{R}^{2 \times 3}$ is defined as follows:

$$B \triangleq \begin{bmatrix} b_1 & -b_2 \frac{\partial \phi_6}{\partial x_2} & -b_3 \frac{\partial \phi_6}{\partial x_3} \\ b_1 \frac{\partial y}{\partial x_1} & b_2 \frac{\partial y}{\partial x_2} & b_3 \frac{\partial y}{\partial x_3} \end{bmatrix}. \tag{22}$$

Based on the open-loop error system represented by (21), we propose a coordinating control strategy for $u(t)$ which drives the hydrogen mass flow rate $y(t)$ to $y_d(t)$ and $P_{\mathrm{asm}}(t)$ to follow a desired ASM pressure trajectory $\phi_6(t)$ ($\phi_6(t)$ in (18) is designed such that $T_{\mathrm{atr}}(t)$ tracks a desired ATR temperature when $P_{\mathrm{asm}}(t)$ follows $\phi_6(t)$). Specifically, the control input $u(t)$ is designed as follows:

$$u = -B^+ \left(\begin{bmatrix} k_1 e_1 \\ k_2 e_2 \end{bmatrix} + N \right) + (I_3 - B^+ B) u_{NB} \tag{23}$$

where k_1, k_2 are positive control gains, $I_j \in \mathbb{R}^{j \times j}$ is an identity matrix, and $B^+(t) \triangleq B^T (BB^T)^{-1} \in \mathbb{R}^{3 \times 2}$ is a pseudo-inverse of $B(t)$ with following properties:

$$BB^+ = I_2 \qquad B(I_3 - B^+ B) = \begin{bmatrix} 0 & 0 & 0 \\ 0 & 0 & 0 \end{bmatrix}. \tag{24}$$

In (23), $u_{NB}(t) \in \mathbb{R}^3$ is an auxiliary control input which is utilized to satisfy the positiveness of $u(t)$ and other control purposes if they are required. Based on (21), (23), and the second equation of (24), it is clear that u_{NB} will not affect the closed-loop system.

Remark 3: The control design in (23) requires that $B(t)$ is full rank. To check the rank of $B(t)$, row operation can be performed to $B(t)$ in (22) as follows:

$$B' \triangleq \begin{bmatrix} b_1 & -b_2 \frac{\partial \phi_6}{\partial x_2} & -b_3 \frac{\partial \phi_6}{\partial x_3} \\ 0 & b_2 \frac{\partial y}{\partial x_2} + b_2 \frac{\partial y}{\partial x_1} \frac{\partial \phi_6}{\partial x_2} & b_3 \frac{\partial y}{\partial x_3} + b_3 \frac{\partial y}{\partial x_1} \frac{\partial \phi_6}{\partial x_3} \end{bmatrix}. \tag{25}$$

From (25) and the fact that $\mathrm{rank}(B) = \mathrm{rank}(B')$, it is clear that $B(t)$ is rank one only if $(\partial y / \partial x_2 + (\partial y / \partial x_1)(\partial \phi_6 / \partial x_2))$ and $(\partial y / \partial x_3 + (\partial y / \partial x_1)(\partial \phi_6 / \partial x_3))$ are both zero. For this highly nonlinear fuel reforming system, it is verified numerically using the algorithm described in Appendix C that $B(t)$ is of rank two when $x \in \mathcal{D}$ and $T_{\mathrm{atr}}^*(t), \dot{T}_{\mathrm{atr}}^*(t)$ are bounded where $\mathcal{D}$ is a compact space. The same numerical verification algorithm can also be utilized to search for the maximum feasible state space of a specific ATR fuel reforming system.

B. Stability Analysis

After substituting (23) into (21), the closed-loop error system can be obtained as follows:

$$\begin{bmatrix} \dot{e}_1 \\ \dot{e}_2 \end{bmatrix} = - \begin{bmatrix} k_1 e_1 \\ k_2 e_2 \end{bmatrix} \tag{26}$$

where (24) has been utilized.

After taking the time derivative of the third equation in (17), the dynamics of $e_3(t)$ can be expressed as follows:

$$\dot{e}_3 = -k_{\mathrm{atr}} e_3 + \phi_7(\cdot) \tag{27}$$

where (9), (11), the first equation of (17), and (18) were utilized. In (27), $\phi_7 \triangleq b_5 K_{\mathrm{air}} e_1 - b_5 g_{\mathrm{out}}(\cdot)$. Since the feasible state space is a compact set, all closed-loop signals are bounded when $x \in \mathcal{D}$. Therefore, it is trivial to assume that

$$|\phi_7(t)| \leqslant \delta \quad \forall x \in \mathcal{D} \tag{28}$$

where δ is a positive constant.

To show the convergence of the closed-loop errors, we assume that $x(0) \in \mathcal{D}$. Let $V(t) \in \mathbb{R}$ denote a non-negative function defined as follows:

$$V = \frac{1}{2} \sum_{i=1}^{3} e_i^2. \tag{29}$$

After taking the time derivative of (29) and then substituting for the closed-loop error systems developed in (26) and (27), the following expression can be obtained:

$$\dot{V} \leqslant -k_1 e_1^2 - k_2 e_2^2 - k_{\mathrm{atr}} e_3^2 + |e_3| |\phi_7|$$

where (28) has been applied. After selecting $k_{\mathrm{atr}} = k_3 + \rho$, where $k_3, \rho > \epsilon > 0$, and applying the nonlinear damping[24], $\dot{V}(t)$ can be upper-bounded as follows:

$$\dot{V} \leqslant -k \sum_{i=1}^{3} e_i^2 + \frac{\delta^2}{4\rho} \tag{30}$$

where $k \triangleq \min\{k_1, k_2, k_3\}$. After substituting (29) into (30), $\dot{V}(t)$ can be expressed as follows:

$$\dot{V} \leqslant -2kV + \frac{\delta^2}{4\rho}. \tag{31}$$

The differential inequality in (31) can be solved to obtain an upper-bound of $V(t)$ as follows:

$$V(t) \leqslant V(0) \exp(-2kt) + \frac{\delta^2}{8\rho k}(1 - \exp(-2kt)) \quad (32)$$

where [25, Lemma 3.2.4] was utilized. From (29) and (32), it is clear that

$$\sum_{i=1}^{3} e_i^2 \leqslant \beta_0 \exp(-2kt) + \beta_1(1 - \exp(-2kt)) \quad (33)$$

where $\beta_0 \triangleq \sum_{i=1}^{3} e_i^2(0), \beta_1 \triangleq \delta^2/4k\rho$. Standard signal chasing can be performed to show all closed-loop signals remain bounded. Therefore, the proposed algorithm achieves local uniformly ultimately bounded tracking. Since $\lim_{\rho \to \infty} \beta_1 = 0$, β_1 can be made arbitrarily small with large enough ρ. This allows us to drive β_1 to any arbitrarily small residue set thus ensuring that the ultimate bound on $(y - y_d)$ and $(T_{atr} - T_{atr}^*)$ can be made arbitrarily small.

Unknown modeling error and measurement noise can usually be considered as additive terms to the system dynamic model. Based on the assumption that the modeling error and measurement noise are bounded, these additional bounded terms can be included into δ in (28) for the dynamic subsystem represented by (27). It is clear that these additional terms introduced by the modeling error and measurement noise will not affect the above stability analysis. For the dynamic subsystem represented by (26), additional bounded terms will be added to the right hand side of (26). Similar to the dynamic subsystem represented by (27), the errors $e_1(t)$ and $e_2(t)$ in (26) will converge to a neighborhood around the origin instead of the origin. Hence, our proposed algorithm is robust to the additive bounded modeling error and measurement noise. For this highly nonlinear system, stability and convergence analyses are limited for control design by linearization compared with the above nonlinear control. Online identification of the linearized dynamics of the air supply manifold, mixer, and autothermal reformer separately using system identification approaches can be applied with standard regulator control design. But either computational effort or switching between two different linearized models will have to be addressed to combine linear control with online identification for this problem. Furthermore, it is well-known that linear controllers have limited operating range on these highly nonlinear systems[26].

IV. SIMULATION RESULTS

To illustrate the performance of the proposed desired trajectory $\phi_6(t)$ and the controller given in (23), numerical simulations will be performed for both the load step-down and step-up operations at a steady state ATR operating temperature. The system parameters are selected as follows:

$$P_{next} = 600 \text{ kPa}$$
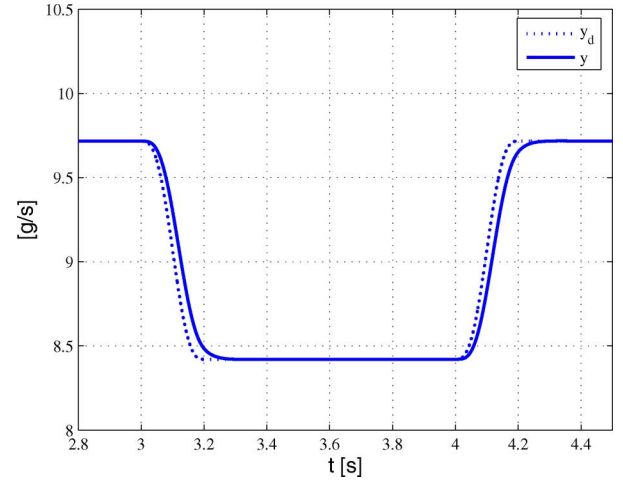$$R = 8.314 \text{ J} \cdot \text{mol}^{-1} \cdot \text{K}^{-1}$$
$$T_{mix} = 500 \text{ K}$$

Fig. 4. Desired and actual hydrogen mass flow rates.

$$V_{mix} = 0.032 \text{ m}^3$$
$$\alpha_m = 0.87 \text{ g} \cdot \text{Pa} \cdot \text{s}^{-1}$$
$$T_{asm} = 400 \text{ K}$$
$$V_{asm} = 0.02 \text{ m}^3$$
$$\alpha_a = 0.21 \text{ g} \cdot \text{Pa} \cdot \text{s}^{-1}$$
$$V_{atr} = 0.028 \text{ m}^3$$
$$\alpha_{out} = 0.17 \text{ g} \cdot \text{Pa} \cdot \text{s}^{-1}$$
$$m_c = 20 \text{ kg}$$
$$c_c = 0.5 \text{ J} \cdot \text{g}^{-1} \cdot \text{K}^{-1}.$$

In our simulation, the desired hydrogen mass flow rate, instead of a power demand or a current demand, is selected as a demand. Equation (13) can be applied to relate the desired hydrogen mass flow rate to a current demand when a specific fuel cell stack is connected to the ATR fuel reforming system. Step-down and step-up commands are smoothed before they are applied to $y_d(t)$. The control gains and the desired ATR operating temperature are selected as follows

$$K = \text{diag}\{80, 80\}, \quad k_{atr} = 140, \quad T_{atr}^* = 1000 \text{ K}.$$

The control gains are selected by a standard try-and-error method as shown in [27]. Based on the configuration of our simulation, the positiveness of the elements of u in (23) can still be satisfied when we choose the auxiliary control input $u_{NB}(t)$ as a zero vector. The desired and actual hydrogen mass flow rates are depicted in Fig. 4. The temperature of the ATR is depicted in Fig. 5. From Fig. 5, it is clear that the residual error in $e_3(t)$ is very small which can be further reduced by increasing β_1 as we showed in (33). Fig. 5 shows the small temperature perturbation due to the smoothed change of the desired hydrogen production flow not the step change of the temperature set point. It does not depict the time constant of the ATR (The time constant for the ATR temperature depends on not only the thermal mass but also the total enthalpy flow $g_{out}(\cdot)$ since $g_{out}(\cdot)$ is a function of the ATR temperature).
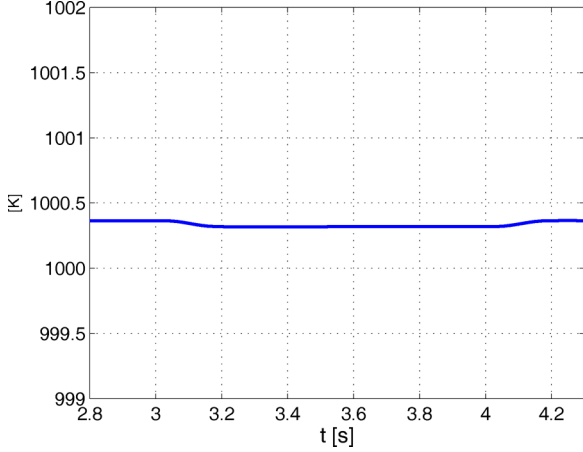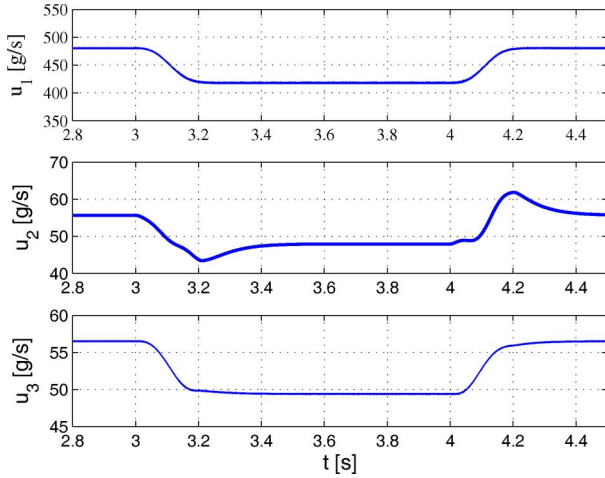
Fig. 5. Temperature of the ATR.

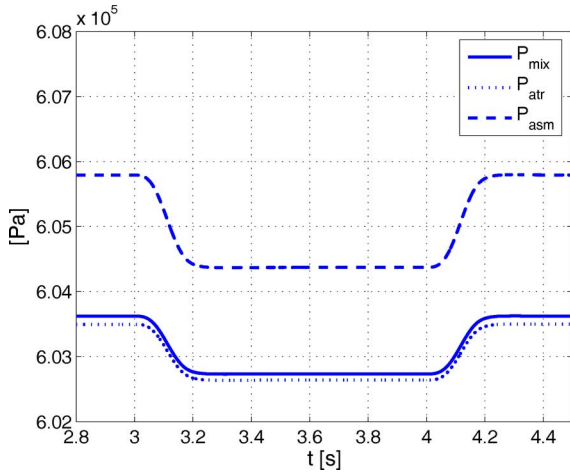Fig. 6. Mass flow rates of air, fuel, and steam.

Fig. 7. Pressures of the HEX, the MIX, and the ATR.

The simulation results validate our control performance which achieves local uniformly ultimately bounded tracking. The mass flow rates of air, fuel, and steam are depicted in Fig. 6. The pressures of the ASM, the MIX, and the ATR are depicted

in Fig. 7. Figs. 4 and 5 show that the proposed controller can track load changes while maintaining the ATR operating temperature.

V. CONCLUSION

A control oriented nonlinear model is developed for an ATR fuel reforming system. The control design fully explores the nonlinearities and the structure of the system dynamic model. Specifically, a pseudo-inverse technique is applied along with the proposed desired pressure for the ASM to coordinate the three input flow rates to control both the hydrogen mass flow rate and the temperature of the ATR. Stability analysis is provided to show a local uniformly ultimately bounded tracking result. Simulation results are provided to demonstrate the performance of the developed controller for the ATR fuel reforming system. Future control work will be focused on incorporating the valve and air compressor dynamics into the fuel processing system model and investigating the region of attraction in terms of the initial states and the control gains. On the modeling aspect, experimental validation of the model can be pursued as the next step to identify opportunities to revisit the model assumptions and to improve its fidelity.

APPENDIX A
PARTIAL DERIVATIVES OF y

$$\frac{\partial y}{\partial x_1} = \frac{y\lambda_{o2f}}{\bar{n}_{H_2}\left(P_{asm} - P_{atr}\right)}\frac{\partial \bar{n}_{H_2}}{\partial \lambda_{o2f}} \quad \frac{\partial y}{\partial x_5} = \frac{y}{\bar{n}_{H_2}}\frac{\partial \bar{n}_{H_2}}{\partial T_{atr}} \quad (34)$$

$$\frac{\partial y}{\partial x_2} = \frac{y}{P_{fuel}^{mix}} + \frac{y}{P_{fuel}^{mix} + P_{st}^{mix} - P_{atr}} \quad (35)$$
$$- \frac{yM_{fuel}}{M_{fuel}P_{fuel}^{mix} + M_{st}P_{st}^{mix}} - \frac{\partial \bar{n}_{H_2}}{\partial \lambda_{s2f}}\frac{y\lambda_{s2f}}{\bar{n}_{H_2}P_{fuel}^{mix}}$$
$$- \frac{\partial \bar{n}_{H_2}}{\partial \lambda_{o2f}}\frac{y\lambda_{o2f}}{\bar{n}_{H_2}\left(P_{fuel}^{mix} + P_{st}^{mix} - P_{atr}\right)}$$
$$- \frac{\partial \bar{n}_{H_2}}{\partial \lambda_{o2f}}\frac{y\lambda_{o2f}}{\bar{n}_{H_2}P_{fuel}^{mix}}$$
$$+ \frac{\partial \bar{n}_{H_2}}{\partial \lambda_{o2f}}\frac{y\lambda_{o2f}M_{fuel}}{\bar{n}_{H_2}\left(M_{fuel}P_{fuel}^{mix} + M_{st}P_{st}^{mix}\right)}$$

$$\frac{\partial y}{\partial x_3} = \frac{y}{P_{fuel}^{mix} + P_{st}^{mix} - P_{atr}} - \frac{yM_{st}}{M_{fuel}P_{fuel}^{mix} + M_{st}P_{st}^{mix}}$$
$$+ \frac{\partial \bar{n}_{H_2}}{\partial \lambda_{s2f}}\frac{y\lambda_{s2f}}{\bar{n}_{H_2}P_{st}^{mix}}$$
$$- \frac{yM_{st}}{M_{fuel}P_{fuel}^{mix} + M_{st}P_{st}^{mix}} + \frac{\partial \bar{n}_{H_2}}{\partial \lambda_{s2f}}\frac{y\lambda_{s2f}}{\bar{n}_{H_2}P_{st}^{mix}}$$
$$- \frac{\partial \bar{n}_{H_2}}{\partial \lambda_{o2f}}\frac{y\lambda_{o2f}}{\bar{n}_{H_2}\left(P_{fuel}^{mix} + P_{st}^{mix} - P_{atr}\right)}$$
$$- \frac{\partial \bar{n}_{H_2}}{\partial \lambda_{o2f}}\frac{yM_{st}\lambda_{o2f}}{\bar{n}_{H_2}\left(M_{fuel}P_{fuel}^{mix} + M_{st}P_{st}^{mix}\right)}$$

$$\frac{\partial y}{\partial x_4} = \frac{y\lambda_{o2f}}{\bar{n}_{H_2}\left(P_{fuel}^{mix} + P_{st}^{mix} - P_{atr}\right)}\frac{\partial \bar{n}_{H_2}}{\partial \lambda_{o2f}}$$
$$- \frac{y}{P_{fuel}^{mix} + P_{st}^{mix} - P_{atr}} - \frac{y\lambda_{o2f}}{\bar{n}_{H_2}\left(P_{asm} - P_{atr}\right)}\frac{\partial \bar{n}_{H_2}}{\partial \lambda_{o2f}}. \quad (36)$$

APPENDIX B
PARTIAL DERIVATIVES OF ϕ_6

$$\frac{\partial \phi_6}{\partial x_2} = \frac{W_{\text{mix}} M_{\text{fuel}} M_{st} P_{st}^{\text{mix}} (K_{st} - K_{\text{fuel}})}{K_{\text{air}} \left(M_{\text{fuel}} P_{\text{fuel}}^{\text{mix}} + M_{st} P_{st}^{\text{mix}} \right)^2} \tag{37}$$
$$- \frac{\alpha_m}{K_{\text{air}}} \left(x_{\text{fuel}}^{\text{mix}} K_{\text{fuel}} + x_{st}^{\text{mix}} K_{st} \right)$$

$$\frac{\partial \phi_6}{\partial x_3} = \frac{W_{\text{mix}} M_{\text{fuel}} M_{st} P_{\text{fuel}}^{\text{mix}} (K_{\text{fuel}} - K_{st})}{K_{\text{air}} \left(M_{\text{fuel}} P_{\text{fuel}}^{\text{mix}} + M_{st} P_{st}^{\text{mix}} \right)^2}$$
$$- \frac{\alpha_m}{K_{\text{air}}} \left(x_{\text{fuel}}^{\text{mix}} K_{\text{fuel}} + x_{st}^{\text{mix}} K_{st} \right)$$

$$\frac{\partial \phi_6}{\partial x_4} = \frac{\alpha_m}{K_{\text{air}}} \left(x_{\text{fuel}}^{\text{mix}} K_{\text{fuel}} + x_{st}^{\text{mix}} K_{st} \right) + 1$$

$$\frac{\partial \phi_6}{\partial x_5} = - \frac{k_{\text{atr}}}{m_5 K_{\text{air}}}. \tag{38}$$

APPENDIX C
THE RANK OF B

To check the rank of B within a feasible state space, we propose a numerical verification algorithm for our ATR fuel reforming system as follows.

- Set $T_{\text{atr}}^* = 1000$ K and set the ATR temperature range from $T_{\text{atr}} = 800$ K to 1200 K with a step of 50 K.
- Set the fuel partial pressure in the mixer $P_{\text{fuel}}^{\text{mix}} = 4 \times 10^4$ Pascal to 8×10^4 Pascal with a step of 2×10^3 Pascal.
- Set $\lambda_{s2f} = 2.5$ to 17.5 with a step of 1. Based on (5) and (10), $P_{st}^{\text{mix}} = \lambda_{s2f} P_{\text{fuel}}^{\text{mix}}$.
- Set $P_{\text{atr}} = \left(P_{\text{fuel}}^{\text{mix}} + P_{st}^{\text{mix}} - 1 \times 10^5 \right)$ to $\left(P_{st}^{\text{mix}} + P_{\text{fuel}}^{\text{mix}} - 100 \right)$ with a step of 4×10^3 Pascal.
- Set $\lambda_{o2f} = 4.5$ to 11 with a step of 1. Based on (2), (4), and (10),

$$P_{\text{asm}} = \frac{\alpha_m M_{\text{O}_2} \lambda_{o2f} x_{\text{fuel}}^{\text{mix}}}{0.2095 M_{\text{fuel}} \alpha_a} (P_{\text{fuel}}^{\text{mix}} + P_{st}^{\text{mix}} - P_{\text{atr}}) + P_{\text{atr}}.$$

- Calculate B based on (34)–(38), then verify the rank of B.

As we simulated based on the above algorithm, the B matrices are always full rank.

ACKNOWLEDGMENT

REFERENCES

[1] S. C. Singhal and K. Kendall, *High Temperature Solid Oxide Fuel Cells*. Amsterdam, The Netherlands: Elsevier, 2003.

[2] Y. Inui, T. Matsumae, H. Koga, and K. Nishiura, "High performance SOFC/GT combined power generation system with CO_2 recovery by oxygen combustion method," *Energy Conv. Manag.*, vol. 46, no. 11-12, pp. 1837–1847, 2005.

[3] B. F. Hagh, "Optimization of autothermal reactor for maximum hydrogen production," *Int. J. Hydrogen Energy*, vol. 28, no. 12, pp. 1369–1377, 2003.

[4] Y. Chen, H. Xu, X. Jin, and G. Xiong, "Integration of gasoline prereforming into autothermal reforming for hydrogen production," *Catalysis Today*, vol. 116, no. 3, pp. 334–340, 2006.

[5] J. Larminie and A. Dicks, *Fuel Cell Systems Explained*, 2nd ed. New York: Wiley, 2003.

[6] F. Rosa, E. Lóopez, Y. Briceño, D. Sopeña, R. M. Navarro, M. C. Alvarez-Galván, J. L. G. Fierro, and C. Bordons, "Design of a diesel reformer coupled to a PEMFC," *Catalysis Today*, vol. 116, no. 3, pp. 324–333, 2006.

[7] J. Pasel, J. Meißner, Z. Porš, C. Palm, P. Cremer, R. Peters, and D. Stolten, "Hydrogen production via autothermal reforming of diesel fuel," *Fuel Cells*, vol. 4, no. 3, pp. 225–230, 2004.

[8] V. Tsourapas, J. Sun, and A. Nickens, "Modeling and dynamics of an autothermal JP5 reformer for marine fuel cell applications," in *Proc. Int. Conf. Efficiency, Cost, Opt., Simulation Environ. Impact Energy Syst.*, Crete, Greece, Jul. 2006, pp. 1419–1426.

[9] D. Papadias, S. H. D. Lee, and D. J. Chmielewski, "Autothermal reforming of gasoline for fuel cell applications: A transient reactor model," *Ind. Eng. Chem. Res.*, vol. 45, pp. 5841–5858, 2006.

[10] J. T. Pukrushpan, A. Stefanopoulou, and H. Peng, *Control of Fuel Cell Power System: Principles, Modeling, Analysis and Feedback Design*. New York: Springer, 2004.

[11] J. T. Pukrushpan, A. G. Stefanopoulou, S. Varigonda, L. M. Pedersen, S. Ghosh, and H. Peng, "Control of natural gas catalytic partial oxidation for hydrogen generation in fuel cell applications," *IEEE Trans. Control Syst. Technol.*, vol. 13, no. 1, pp. 3–14, Jan. 2005.

[12] J. E. Slotine and W. Li, *Applied Nonlinear Control*. Englewood Cliffs, NJ: Prentice-Hall, 1991.

[13] Y. Hu, D. J. Chmielewski, and D. Papadias, "Autothermal reforming of gasoline for fuel cell applications: Controller design and analysis," *J. Power Sources*, vol. 182, pp. 298–306, 2008.

[14] L. Menini, L. Zaccarian, and C. Abdallah, *Current Trends in Nonlinear Systems and Control*. Cambridge, MA: Birkhäuser, 2006.

[15] B. Ariyur and M. Krstic, *Real-Time Optimization by Extremum-Seeking Control*. New York: Wiley-Interscience, 2003.

[16] C. Wang, "Fundamental models for fuel cell engineering," *Chem. Rev.*, vol. 104, pp. 4727–4766, 2004.

[17] H. Xi, "Dynamic modeling and control of planar SOFC power systems," Ph.D. dissertation, Dept. Naval Arch. Marine Eng., Univ. Michigan, Ann Arbor, 2007.

[18] C. Bao, K. Zhang, M. Ouyang, B. Yi, and P. Ming, "Dynamic test and real-time control platform of anode recirculation for PEM fuel cell systems," *J. Fuel Cell Sci. Technol.*, vol. 3, pp. 333–345, 2006.

[19] C. D. Rakopoulos, D. T. Hountalas, and D. C. Rakopoulos, "Comparative environmental evaluation of JP-8 and diesel fuels burned in direct injection (DI) or indirect injection (IDI) diesel engines and in a laboratory furnace," *Energy Fuels*, vol. 18, pp. 1302–1308, 2004.

[20] J. Sun and I. Kolmanovsky, "Load governor for fuel cell oxygen starvation protection: A robust nonlinear reference governor," *IEEE Trans. Control Syst. Technol.*, vol. 13, no. 6, pp. 911–920, Nov. 2005.

[21] F. Zenith and S. Skogestad, "Control of fuel cell power output," *J. Process Control*, vol. 17, pp. 333–347, 2007.

[22] M. Arcak, H. Görgün, L. M. Pedersen, and S. Varigonda, "A nonlinear observer design for fuel cell hydrogen estimation," *IEEE Trans. Control Syst. Technol.*, vol. 12, no. 1, pp. 101–110, Jan. 2004.

[23] F. Zenith and S. Skogestad, "Control of the mass and energy dynamics of polybenzimidazole-membrane fuel cells," *J. Process Control*, vol. 19, pp. 415–432, 2009.

[24] H. K. Khalil, *Nonlinear Systems*, 3rd ed. Englewood Cliffs, NJ: Prentice-Hall, 2002.

[25] P. A. Ioannou and J. Sun, *Robust Adaptive Control*. Englewood Cliffs, NJ: Prentice-Hall, 1996.

[26] M. Serra, J. Aguado, X. Ansede, and J. Riera, "Controllability analysis of decentralised linear controllers for polymeric fuel cells," *J. Power Sources*, vol. 151, pp. 93–102, 2005.

[27] J. Chen, W. E. Dixon, D. M. Dawson, and M. McIntire, "Homography-based visual servo tracking control of a wheeled mobile robot," *IEEE Trans. Robotics*, vol. 22, no. 2, pp. 407–416, Apr. 2006.

Jian Chen (M'06) received the B.E. degree in testing technology and instrumentation and the M.E. degree in control science and engineering Zhejiang University, Hangzhou, P.R. China, in 1998 and 2001, respectively, and the Ph.D. degree in electrical engineering from Clemson University, Clemson, SC, in 2005.

After completing the Ph.D. program in August of 2005, he had worked on MEMS as a Research Associate for one year and then he worked on fuel cell modeling and control at the University of Michigan, Ann Arbor for one and a half years. Now he works on fuel cell power system modeling and control at IdaTech LLC, Bend, OR. His research interests include fuel cell modeling and control, MEMS, visual servo techniques, nonlinear control, and multi-vehicle navigation.

Jing Sun (F'04) received the Ph.D degree from the University of Southern California, Los Angeles, in 1989, and the B.S. and M.S. degrees from University of Science and Technology of China, Hefei, China, in 1982 and 1984, respectively.

From 1989–1993, she was an Assistant Professor with the Electrical and Computer Engineering Department, Wayne State University. She joined Ford Research Laboratory in 1993 where she worked in the Powertrain Control Systems Department. After spending almost 10 years in industry, she came back to academia and joined the faculty of the College of Engineering at University of Michigan, Ann Arbor, in 2003, where she is now a professor in the Department of Naval Architecture and Marine Engineering and Department of Electrical Engineering and Computer Science. Her research interests include system and control theory and its applications to marine and automotive propulsion systems. She holds over 30 U.S. patents and has coauthored a textbook on robust adaptive control.

Dr. Sun was a recipient of the 2003 IEEE Control System Technology Award.